Int. J. Electrochem. Sci., 13 **(2018)** 8440 – 8453, doi: 10.20964/2018.09.33

International Journal of
ELECTROCHEMICAL
SCIENCE
www.electrochemsci.org

Oxygen-rich Hierarchical Porous Carbon Derived from Coal Tar Pitch for Superior Electric Double Layer Capacitor Application

Qi-Qi Zhuang, Jing-Pei Cao[*], *Zhi-Qiang Hao, Xiao Wan, Yan Wu, Zhong-Hai Ni, Xiao-Yan Zhao*[**], *Xian-Yong Wei*

Key Laboratory of Coal Processing and Efficient Utilization (Ministry of Education), China University of Mining & Technology, Xuzhou 221116, Jiangsu, China
[*]E-mail: caojingpei@cumt.edu.cn
[**]E-mail: zhaoxiaoyan@cumt.edu.cn

Received: 15 May 2018 / *Accepted:* 28 June 2018 / *Published:* 5 August 2018

Coal tar pitch (CTP) with a great deal of polynuclear aromatic structural units is a potential precursor for preparing porous carbon. In this paper, CTP was selected as raw material, and oxygen-rich hierarchical porous carbon (OHPC) was prepared successfully by facile one-step KOH activation, which was attributed to the H_2O oxidation during this process. The oxygen content in hierarchical porous carbon was well above the oxygen content in CTP. Besides, possible oxidation mechanism was proposed. The influence of activation temperature and activation ratio (m_{KOH}/m_{CTP}) on the pore structure of OHPC was also investigated, and the largest specific surface area reached 2342 m^2 g^{-1}. When OHPC was applied to electric double layer capacitor in the two electrode system, it shows good electrochemical performance. Its specific capacitance and energy density could reach 308 F g^{-1} and 8.31 Wh kg^{-1} in 6 M KOH solution, respectively. Meanwhile, the capacitance retention of OHPCs was up to 95.4% at 2 A g^{-1} after 10000 cycles. This paper not only provides a simple method of oxygen doping for porous carbon, but also achieve the green and high value-added utilization of CTP.

Keywords: Coal tar pitch; Oxygen-rich hierarchical porous carbon; Steam oxidation; Electric double layer capacitor

1. INTRODUCTION

With the increase in demand for energy storage, the development and utilization of clean and renewable energy are the problem to be solved urgently [1]. Electric double layer capacitor (EDLC) has caused widely attention owing to their advantages of high power density, low pollution, excellent cycle stability and friendly environment [2-5]. The electrochemical performance of EDLCs strongly

depend on the physicochemical properties of the electrode materials [6, 7]. Porous carbon (PC) materials as the most general electrode materials for EDLCs include activated carbons [8], porous carbon nanotubes [9], carbon sphere and carbon nanofibers [10, 11]. Additionally, PCs have the features of high specific surface area (SSA), low cost, good chemical stability, abundant raw material and superior electrical conductivity [12, 13], but ordinary PCs have the disadvantages of low energy density and poor rate performance. Meanwhile, hierarchical porous carbon (HPC), which has rational pore size distribution (PSD), attracts extensive attention as an ideal carbon-based electrode material for EDLC [2]. Micropores are major contributors for SSA and specific capacitance because of its abundant active site of adsorption, and mesopores promote the diffusion of electrolyte ions as transmission channel; besides, macropores act as ion-buffering to ensure that there are electrolyte ions to enter the electrode material rapidly [14]. Geng [15] prepared two-dimensional hierarchical porous carbon sheets by using nano-MgO sheet as template with KOH activation, and its specific capacitance could reach 290 F g^{-1} with 6 M KOH solution as electrolyte. Han [16] used a simple and efficient hydrothermal treatment to prepare hierarchical porous carbon hollow-spheres with superior specific capacitance of 270 F g^{-1} in 6 M KOH solution.

Moreover, the energy density of hierarchical porous carbons (HPCs) can be increased by doping heteroatoms. Oxygen as a common heteroatom can improve the surface wettability and generate pseudocapacitance [17, 18]. Feng used oxygen-rich materials (waste dragon fruit skin, Momordica grosvenori skin and Firmiana catkins) to prepare activated carbon. Three kinds of as-prepared activated carbons resulted in capacitances of 286.9 F g^{-1}, 238.7 F g^{-1} and 226.6 F g^{-1} at 0.5 A g^{-1} [19]. Hsieh oxidized polyacrylonitrile-based activated carbon fabric at 250 ^{o}C under an oxygen atmosphere. Due to the treatment, the overall specific capacitance showed an increase up to 25% (e.g., from 120 to 150 F g^{-1} at 0.5 mA cm^{-2}) [20]. The university method of oxygen doping is H_2O_2/HNO_3 oxidation or the utilization of carbon source with rich oxygen [19, 21, 22], which are relatively complicated, costly and dangerous. Hence, it is necessary to find a simple doping method.

Coal tar pitch (CTP) is a residue from coal tar, occupying about 45-50% of the total coal tar [23, 24]. CTP mainly contains plenty of polycyclic aromatic hydrocarbons and heterocyclic compounds [15], so that CTP is an ideal low cost carbon precursor based on their rich carbon content and good cost-efficiency. Furthermore, it can prepare carbon materials with different structures [25-27]. However, its chemical and physical properties can influence their transformation to carbons. The thermal properties of CTP are varied in a wide range and unstable [28, 29]. Therefore, it is interesting and promising to use CTP to prepare OHPC by simple KOH activation [30].

In this study, CTP was selected as the precursor to prepare OHPC through simple one-step KOH activation, and the oxygen content in OHPC was significantly increased. The obtained OHPCs possess high SSA, abundant pore structures and superior electrochemical performance. It not only realized efficient oxygen doping, but also achieved green and high value-added utilization of CTP.

2. MATERIALS AND METHODS

2.1. Materials

CTP obtained from Shandong Energy Zaozhuang Mining Group Co. Ltd. was used as raw material, and other reagents are analytical purity and no other treatments are carried out.

2.2. Preparation of OHPC

The experiment used a simple one-step activation method. CTP was impregnated in KOH solution with the different activation ratios (m_{KOH}/m_{CTP}, 1, 2, 3 and 4). The mixtures were dried at 100 ^{o}C for 8 h, and transferred into a tube furnace. Then, the samples were heat-treated at different activation temperatures (600, 700, 800 and 900 ^{o}C) for 1 h under Ar atmosphere. After activation, the as-prepared crude OHPCs were washed by 2 M HCl and deionized water until the solution showed neutrality. The samples were dried in vacuum oven at 150 ^{o}C for 3 h. The as-prepared OHPC was named OHPC-*y*-*x*, where *y* stood for activation temperature and *x* stood for activation ratio (m_{KOH}/m_{CTP}).

2.3. Characterization

CTP and OHPC were ground and sieved below 200 meshes in order to characterize the sample. In addition, the characterization methods include thermogravimetric analysis (TGA, Mettler-Toledo TGA/DSC1 analyzer), elemental analysis (Vario MACRO Cube elemental analyzer), field emi ssion scanning electron microscopy (FESEM, Merlin Zeiss), X-ray photoelectron spectroscopy (XPS, Thermo ESCALAB 250Xi), and N_2 adsorption-desorption test (Gold APP V-sorb 4800TP surface area and pore size analyzer). Additionally, Brunauer-Emmett-Teller (BET) equation was used to calculate the specific surface area (SSA). The t-plot method was used to obtain the micropore surface area (S_{micro}) and micropore volumes (V_{micro}) and the surface areas and pore volumes of the mesoporous were analyzed according to the Barrette-Joynere-Halenda (BJH) method.

2.4. Electrochemical Measurements

85 wt% of OHPC, 10 wt% of acetylene black and 5 wt% of polytetrafluoroethylene were mixed and grinded for preparing electrodes, and then the mixture was pressed onto nickel foam with a diameter of 13 mm. Two electrodes were assembled in a CR2032 coin cell with 6 M KOH as electrolyte. Galvanostatic charge-discharge (GCD), cyclic voltammetry (CV) and electrochemical impedance spectroscopy (EIS) were tested for investigating electrochemical performance. The characterization of electrode materials was accomplished in the two electrode system. The GCD measurements were carried out at different current densities within the potential window between 0 and 0.9 V through a NEWARE CT-3008-5 V 50 mA-164 battery testing system. The CV and EIS measurements were performed on an Iviumstat Vertex electrochemical workstation. CV was measured in a voltage window between 0 and 0.9 V at different potential scan rates. EIS was accomplished by a frequency range from 10^{6} Hz to 10^{-3} Hz at open circuit voltage with 10 mV amplitude.

The specific capacitance (C_g) was calculated on the basis of the Eq. 1:

$$C_g = 2\frac{I\times\Delta t}{m\times\Delta V} \quad (1)$$

where I (A), ΔV (V), Δt (s) and m (g) is the discharge current, voltage change, discharge time and the mass of active material on a single electrode, respectively.

The energy and power densities of EDLC systems were calculated via the following Eqs. :

$$E = \frac{C_g\times\Delta V^2\times 1000}{2\times 4\times 3600} \quad (2)$$

$$P = \frac{E\times 3600}{\Delta t} \quad (3)$$

where E (Wh kg^{-1}) is energy density, P (W kg^{-1}) is power density, ΔV (V) is the voltage change and Δt (s) is the discharge time.

3. RESULTS AND DISCUSSION

3.1. Structural features

The proximate analysis of CTP is measured under dry base conditions. The contents of ash, volatile, and fixed carbon are 4.49%, 45.19% and 50.32%, respectively. Fig. 1 shows the TG and derivative thermogravimetry (DTG) curves of CTP, and moisture and light components are separated from CTP at the first stage (100-320 ^{o}C). The second stage (320-500 ^{o}C) corresponds to the cross-linking of CTP molecules accompanied by cracking side chains and forming free radicals during pyrolysis process. In the third stage above 500 ^{o}C, undecomposed and unstable carbon result the rate of pyrolysis gradually decreased. It suggests that CTP can decompose from 100 ^{o}C to 900 ^{o}C and the compositions and structures of CTP can influence the pyrolysis process [27, 31, 32].

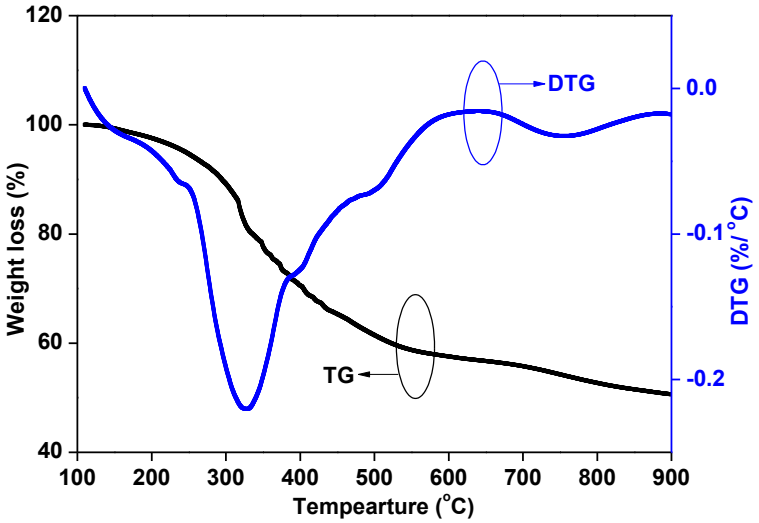

Figure 1. TG-DTG curves of CTP

The SEM images of OHPC-700-2 under different magnifications are shown in Fig. 2. It is obvious that the OHPC-700-2 has abundant pore structure with hierarchical porous structure, which is beneficial to the rapid transfer of electrolyte ions [33].

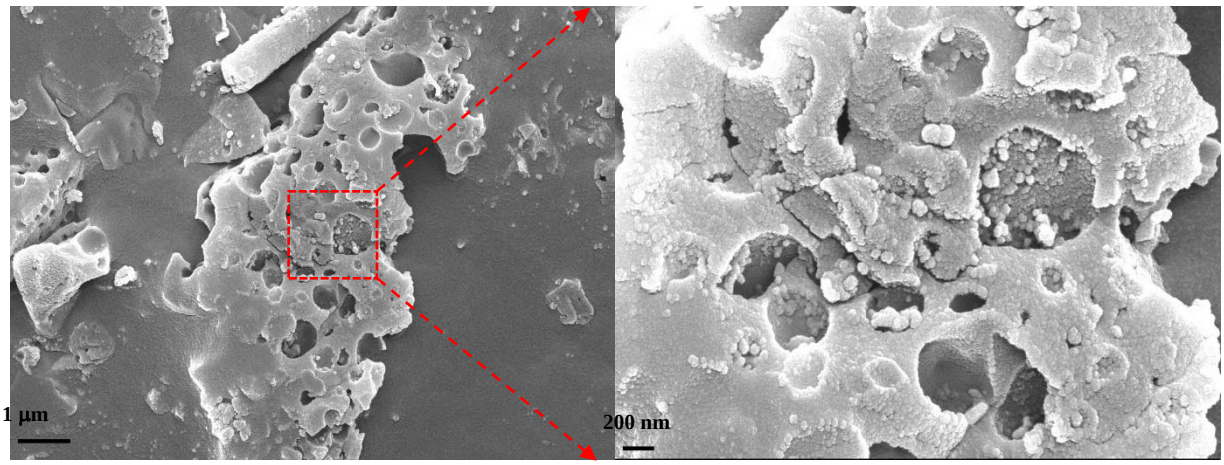

Figure 2. SEM images of OHPC-700-2

As illustrated in Figs. 3a and 3c, the N_2 adsorption-desorption isotherm of OHPC-*x*-*y* possesses the feature of type I isotherm according to IUPAC. It is remarkable that the volume absorbed rose sharply at low relatively pressure (P/P_0, 0.0-0.1), which is due to the existence of abundant micropores. Moreover, these isotherms show slight upward trend from P/P_0 = 0.1 to 0.99 resulting from mesoporous adsorption. These porous carbon materials have interconnected pore structure based on the H4 hysteresis loop [34, 35]. The SSA of OHPC-*x*-2 enhances from 907 to 2086 m^2 g^{-1}, when increasing temperature from 600 to 900 ^oC. The total pore volume can reach 1.2 cm^3 g^{-1} under 900 ^oC (Table 1). However, the micropore surface area of OHPC-*x*-2 decrease significantly when raising the activation temperature from 800 ^oC to 900 ^oC, indicating that the micropores can be converted into mesopores at high temperature [36, 37]. For OHPC-700-*y*, its SSA increases from 642 to 2342 m^2 g^{-1} with the increase in activation ratio. Besides, its H4 hysteresis loop also becomes more apparent, suggesting the increase of mesopore ratio [35, 38-40]. This is since it is conducive to the formation of micropores in the HPCs with the increase of KOH. As shown in Figs. 3b and 3d, the PSD curve of OHPC-*x*-*y* mainly distributed in the range of 0.5-2 nm, which is beneficial to the rapid transfer of ions [41]. Meanwhile, OHPC-*x*-*y* possesses a certain amount of mesopores and macropores (insert of Figs. 3b and 3d), indicating the pore structure of OHPCs is hierarchical porous.

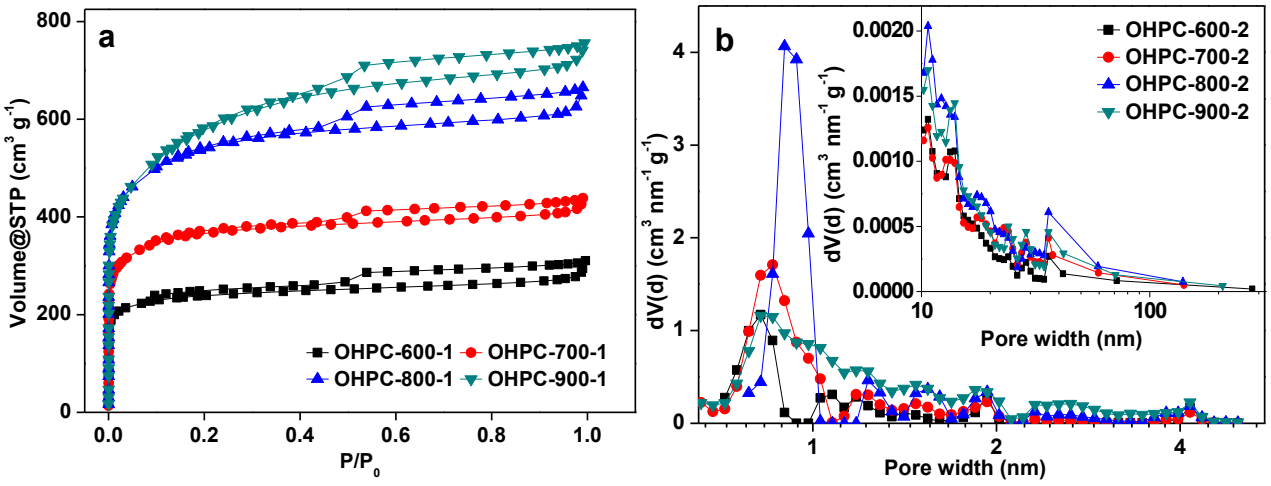

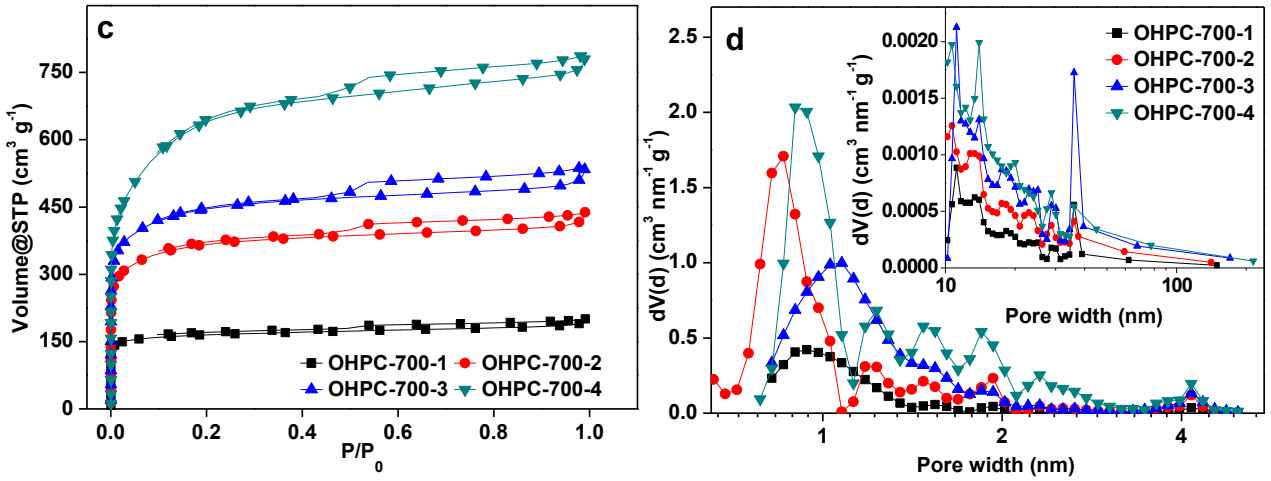

Figure 3. N_2 adsorption-desorption isotherms of OHPC-*y*-2 (a) and OHPC-700-*x* (c) and PSDs of OHPC-*y*-2 (b) and OHPC-700-*x* (d).

Table 1. Textural parameters of OHPCs.

Sample	Y_a[a] (%)	S_{BET}[b] ($m^2\ g^{-1}$)	V_{total}[c] ($cm^3\ g^{-1}$)	S_{micro}[d] ($m^2\ g^{-1}$)	V_{micro}[e] ($cm^3\ g^{-1}$)	D[f] (nm)
OHPC-700-1	55.4	642	0.3	597	0.2	1.93
OHPC-700-2	44.4	1382	0.7	1299	0.5	1.96
OHPC-700-3	35.4	1673	0.8	1571	0.7	2.02
OHPC-700-4	30.3	2342	1.2	2131	0.9	2.10
OHPC-600-2	47.0	907	0.5	840	0.4	2.12
OHPC-700-2	44.4	1382	0.7	1299	0.5	1.96
OHPC-800-2	35.1	1993	1.0	1855	0.8	2.07
OHPC-900-2	30.9	2086	1.2	1801	0.8	2.24

[a] Y_a: The yield of activation.

[b] S_{BET}: Specific surface area from multiple BET method.

[c] V_{total}: Total pore volume at $P/P_0 = 0.99$.

[d] S_{micro}: Micropore surface area.

[e] V_{micro}: Micropore volume.

[f] D: Average pore size.

Furthermore, there are several simultaneous/consecutive reactions in KOH activation process below 700 °C, as shown in below [42, 43]:

$$2KOH \rightarrow K_2O + H_2O \quad (4)$$

$$H_2O + C \rightarrow CO + H_2 \quad (5)$$

$$H_2O + CO \rightarrow CO_2 + H_2 \quad (6)$$

$$CO_2 + K_2O \rightarrow K_2CO_3 \quad (7)$$

KOH dehydrates to K_2O at 400 °C (Eq. 4). Then, the reaction of carbon and H_2O consumes carbon with producing CO and H_2 (Eq. 5) to develop some pores. Subsequently, K_2CO_3 is formed (Eq.

7) by the reaction of K_2O and CO_2 which is produced in the reaction in Eq. 6. Apart from the production of CO and H_2, the reaction between H_2O and carbon material will lead to the oxidation of carbon, so that the oxygen doping can be achieved by one-step KOH activation. Therefore, it is significant that H_2O and CTP will react with each other under a high temperature, leading to the rise in oxygen content of porous carbon material.

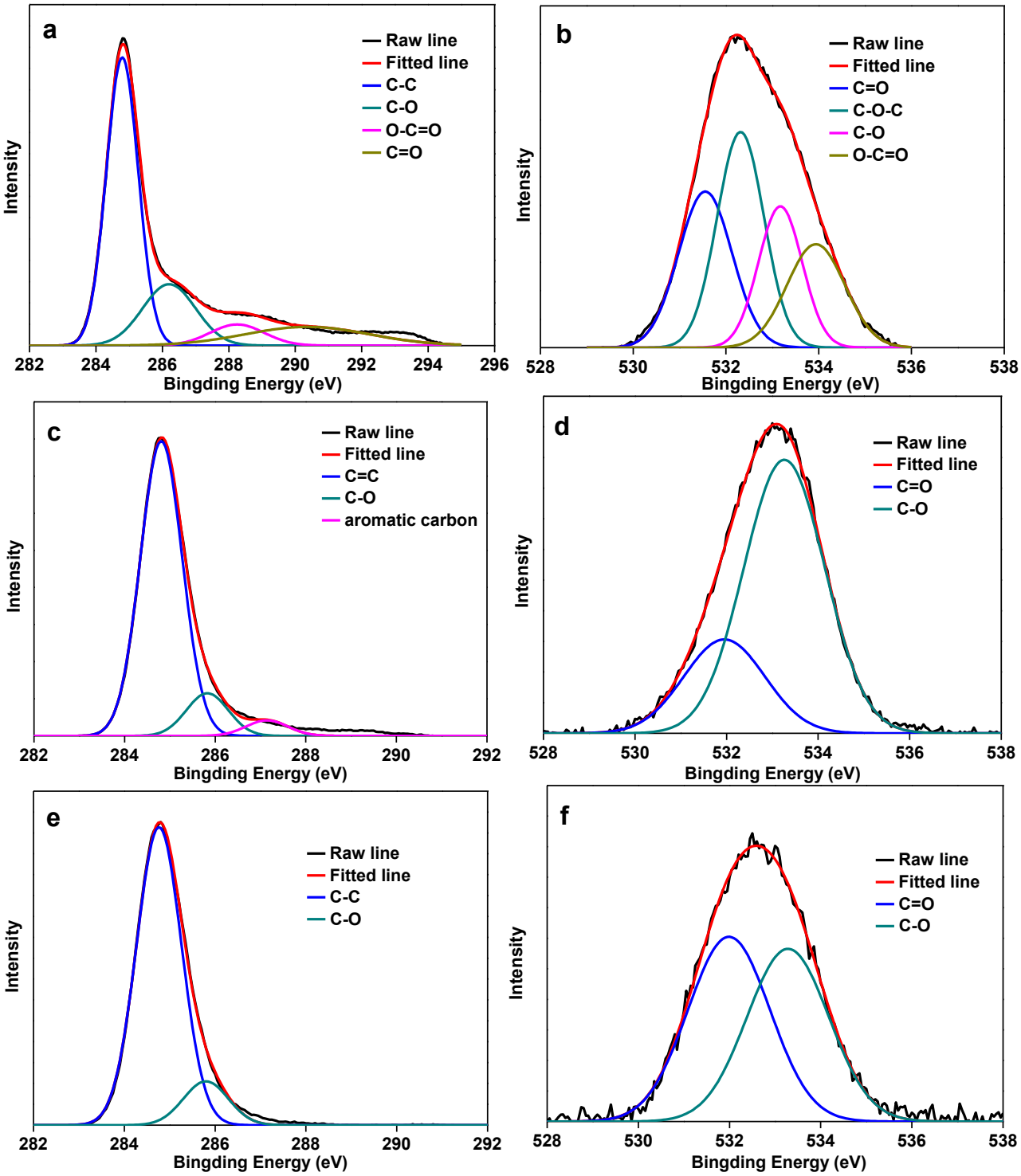

Figure 4. XPS C 1s (a, c and e) and O 1s (b, d and f) peaks of OHPC-700-2, char and CTP.

Table 2. Ultimate and XPS analysis of CTP and OHPC-700-2.

Sample	Ultimate analysis (wt%, daf)					XPS analysis (wt%, daf)	
	C	H	N	S	O*	C 1s	O 1s
CTP	88.6	5.9	2.2	2.4	0.9	88.6	6.2
OHPC-700-2	77.9	0.7	1.4	1.1	18.9	69.4	18.0

XPS and ultimate analysis were carried out for investigating the oxygen contents and oxygen bonding configurations of coke and OHPC-700-2. As shown in Fig. 4a, the high-resolution C 1s spectrum include four peaks of C-C/C=C (284.8 eV), C-O (286.5 eV), O-C=O (288.8 eV) and C=O (289.5 eV) [15, 30]. The four fitted peaks of O 1s XPS spectra are located at 531.5 eV (C=O), 532.4 eV (C-O-C), 533.5 eV (C-O) and 533.8 eV (O-C=O) (Fig. 4b), respectively. The deconvoluted O 1s XPS spectra of char and CTP are composed of 531.9 eV (C=O) and 533.2 eV (C-O) (Figs. 4d and 4f). In general, there are more oxygen-containing functional groups in OHPC compared with char, and the oxygen content is obviously enhanced (Table 2). Additionally, the oxygen content of OHPC-700-2 is higher than that of CTP according to their ultimate and XPS analyses, as listed in Table 2. It illustrates that oxygen is doped successfully by KOH activation. This is mainly due to steam reacting with different chemical state carbons during the activation, so that oxygen-containing functional groups are generated, such as C=O, C-O-C, C-O and O-C=O. The types of oxygen functional groups are changed obviously in comparison with char and CTP. In addition, the change of oxygen-containing functional groups in OHPC-700-2 is not caused by the carbonization of CTP, but by the oxidation of steam based on the XPS results of CTP, Char and OHPC-700-2 (Fig. 4) [44]. After activation, the bonds of C-C and C=C are converted to O-C=O, C=O and C-O (Table 3). The possible oxidation process is shown in Fig. 5.

Table 3. Contents of C1s and O1s of the OHPC-700-2 and char.

Sample	C 1s (%)					O 1s (%)			
	C-C/C=C	C-O	O-C=O	C=O	aromatic C	C=O	C-O-C	C-O	O-C=O
OHPC-700-2	57.8	20.5	7.1	4.6	-	27.3	33.0	20.2	19.5
Char	81.5	13.6	-	-	4.9	32.9	-	67.1	-

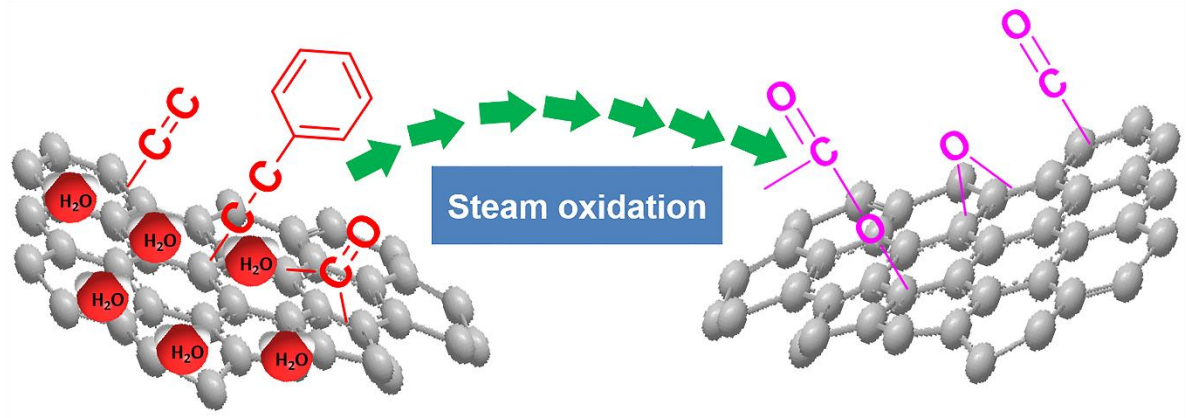

Figure 5. The simple oxidation of steam during KOH activation

Besides, the oxygen-containing functional groups can generate additional pseudocapacitance and enhance the wettability of the porous carbon, so that the specific capacitance and energy density of carbon-based electrode material should be improved [45-47].

3.2. Electrochemical performances

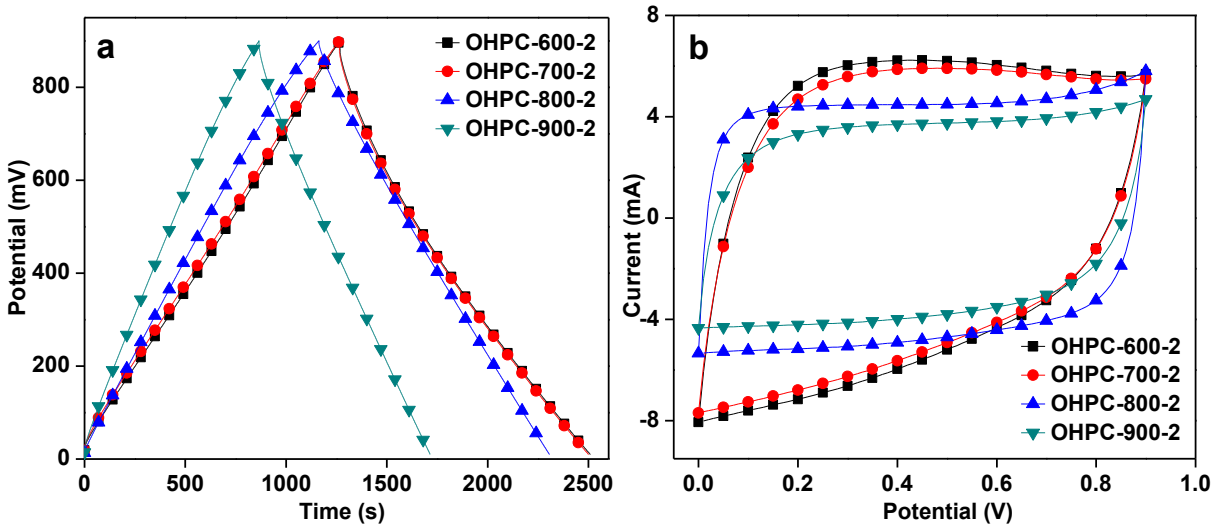

Figure 6. GCD curves of OHPC-*y*-2 at 100 mA g^{-1} (a); CV curves of OHPC-*y*-2 at the scan rate of 5 mV s^{-1} (b).

All the GCD curves of OHPC-*y*-2 at 100 mA g^{-1} present linearity and symmetry (Fig. 6a), which may be owing to the presence of pseudocapacitance and the inexistence of obvious ohmic drops [27, 48]. Moreover, the CV curve of OHPC-700-2 approaches to a quasi-rectangular shape and has the largest area (Fig. 6b), demonstrating the specific capacitance of OHPC-700-2 is the largest [49, 50]. According to Eq. 1, the specific capacitance of OHPC-600-2, OHPC-700-2, OHPC-800-2 and OHPC-900-2 is 302, 308, 284 and 194 F g^{-1}, respectively. Hence, the optional activation temperature is 700 ^{o}C.

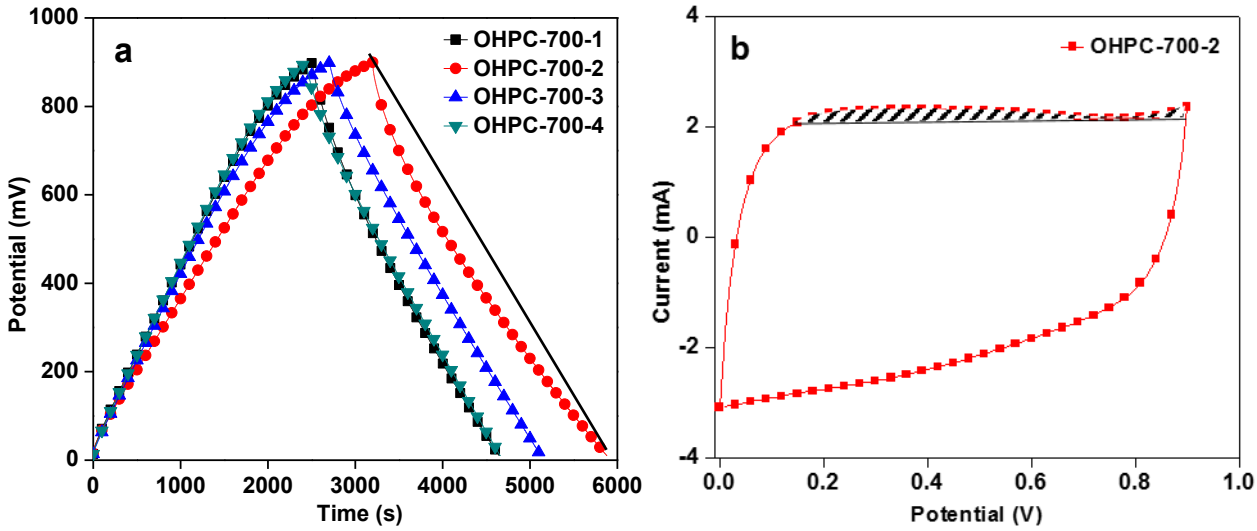

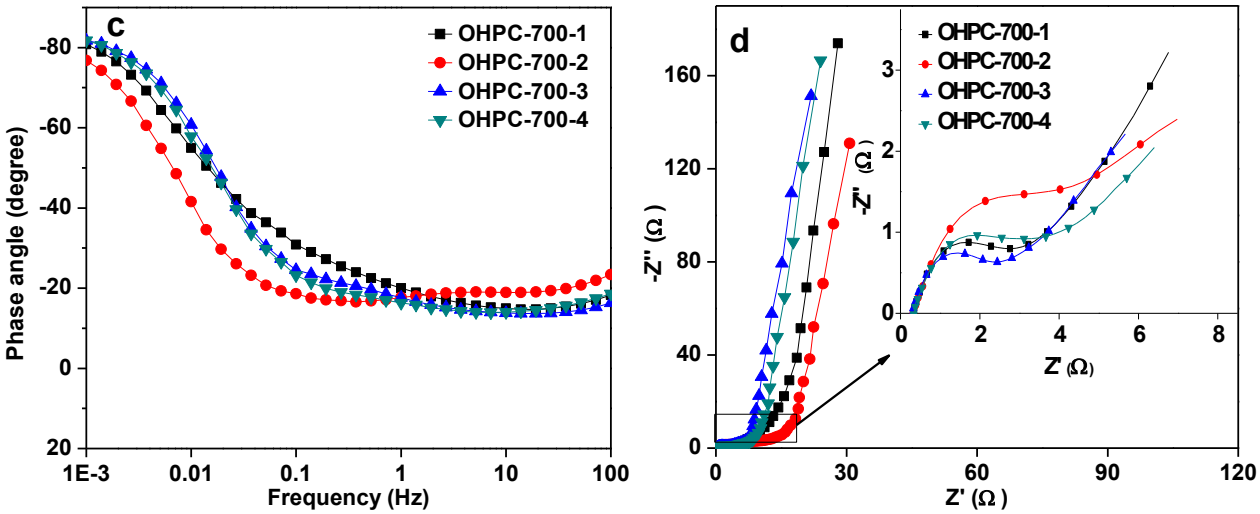

Figure 7. GCD curves of OHPC-700-*x* at 50 mA g^{-1} (a); CV curves of OHPC-700-2 at the scan rate of 2 mV s^{-1} (b); Impedance phase angle versus frequency (c); Nyquist plots of OHPC-700-*x* (d).

Fig. 7a displays the GCD curves of the OHPCs with different activation ratios at 50 mA g^{-1}. All the curves display excellent symmetry, indicating the electrodes prepared from the OHPCs have typical electric double layer capacitive behavior and good reversibility. The discharge time of OHPC-700-2 is longer than others, suggesting that the specific capacitance of OHPC-700-2 is the largest [48, 50]. According to Eq. 4, H_2O originates from KOH activation at high temperature, and abundant oxygen-containing functional groups are also developed. Hence, pseudocapacitance would be generated by according to the following equations [51-53]:

$$OH^- + > C\text{-}OH \leftrightharpoons > C = O + H_2O + e^- \quad (8)$$

$$> C = O + e^- \leftrightharpoons > C\text{-}O^- \quad (9)$$

Meanwhile, oxygen-containing functional groups would provide pseudocapacitance in charge/discharge (the shaded part of Fig. 7b); besides, these groups are propitious to improve the wettability of carbon-based electrode materials. Additionally, the discharge curve is not a straight line, which is also caused by the existence of pseudocapacitance (Fig. 7a) [54]. At low frequency, the phase angles of all OHPCs are close to -90° (Fig. 7c), indicating a capacitive behavior, and reached -45° at the frequency of 0.021, 0.008, 0.023 and 0.019 Hz (f_0) of OHPC-700-1, OHPC-700-2, OHPC-700-3 and OHPC-700-4, respectively. Meanwhile, the corresponding time constant τ_0 ($\tau_0 = 1/f_0$) are 47, 125, 43 and 52 s, respectively [55]. The Nyquist plots of OHPC-700-*x* are exhibited in Fig. 7d. All the OHPC electrodes have similar impedance behaviors. It is obvious that all the curves are approximately vertical lines at low frequency, which indicates the excellent electrochemical capacitive properties [49, 50]. OHPCs show the slope in the 45° portion of the Nyquist curve, which commonly refers to as Warburg resistance in the intermediate frequency. Its presence is due to the resistance of ion diffusion inside the carbon pores [26]. In the high frequency region, the four curves intersection with the real axis represent equivalent series resistance and they have no obvious difference [56]. This is because all of the EDLCs use the 6 M KOH as electrolyte and the method of assembly is the same. As shown in

Fig. 7d, the charge-transfer resistance of OHPC-700-3 is low because the large micropore surface area is conducive to the transport of electrolyte ions inside the electrode material [57, 58].

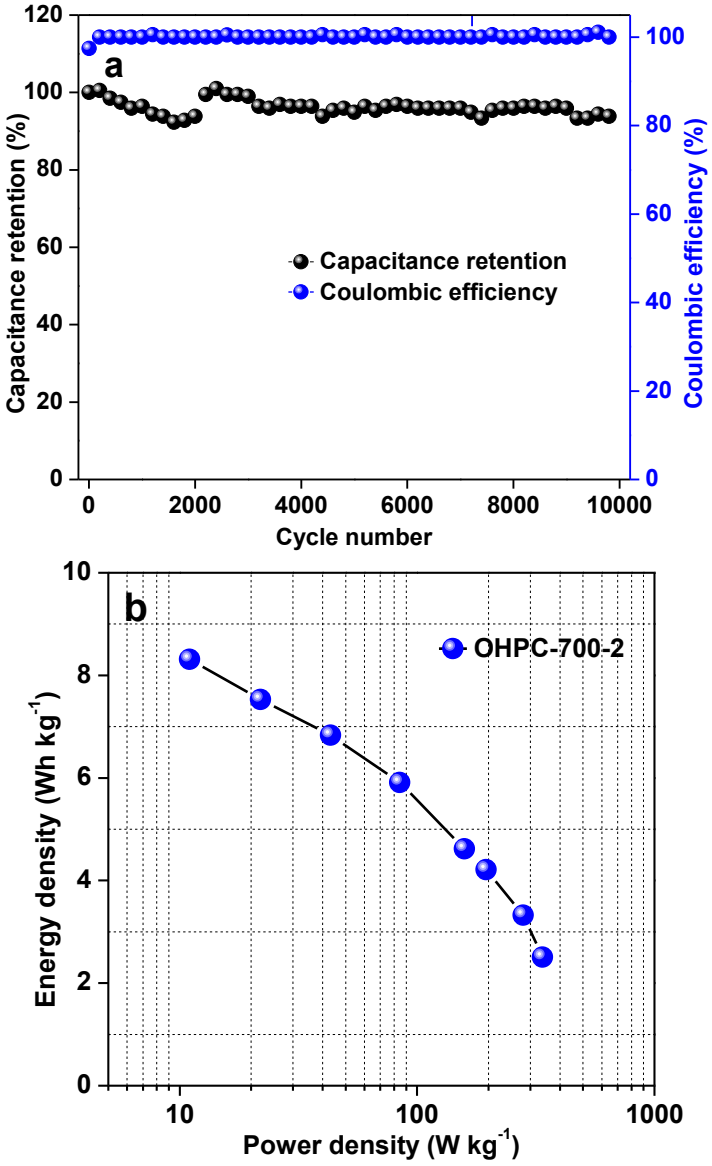

Figure 8. Cycle life of OHPC-700-2 at current density of 2 A g^{-1} (a) and Ragone plot of OHPC-700-2 device at different current density (b).

Cycle life is an important indicator for evaluating EDLC. Fig. 8a displays the cycling performance and coulomb efficiency of OHPC-700-2 under 2 A g^{-1}. The capacitance retention rate increase in the first 250 cycles due to electrolyte ions need enough time to enter the micropores. Then, the capacitance retention rate begins to decline, and remains 95.4% after 10000 cycles, suggesting that OHPC-700-2 has excellent cycling performance and electrochemical stability. In addition, the value of coulomb efficiency can reach 100% after 15 cycles, illustrating the sample has good electrochemical reproducibility. The energy density and power density of OHPC-700-2 are calculated by Eqs. 2 and 3. The energy density and power density are 8.31 Wh kg^{-1} and 11.03 W kg^{-1} at 50 mA g^{-1} (Fig. 8b), respectively.

To compare the performance of the other electrode materials, a summary of performance of other electrode materials is presented in the Table 4. The OHPC prepared in this work exhibits high specific capacitance, suggesting that OHPC prepared by one-step KOH activation is a potential electrode material and show excellent electrochemical performance.

Table 4 Electrode materials for EDLCs.

Raw materials	SSA (m^2 g^{-1})	Cg (F g^{-1})	Electrolyte	Reference
Lignin and lignite	3311	280	6 M KOH	[31]
Glucose	658	270	6 M KOH	[16]
HyperCoal	2540	46	6 M KOH	[58]
oil palm empty fruit bunches	1704	150	1 M H_2SO_4	[39]
Ginkgo shells	1775	178	6 M KOH	[59]
CTP	1382	308	6 M KOH	Present study

4. CONCLUSIONS

In summary, one-step KOH activation as an effective and simple method was developed to prepare OHPC from CTP. The as-obtained OHPC possesses abundant oxygen-containing species and developed pore structure which provides a good channel for the electrolyte ions transport. Based on these features, OHPC-700-2 displays a high specific capacitance (308 F g^{-1} at 0.05 A g^{-1}) and a good retention rate (72.5%). In addition, it also shows outstanding cycling stability with 95.4% specific capacitance retention after 10000 cycles. This work shows that OHPC has great potential as an energy storage device, and it provides a new and simple way for the value-added utilization of CTP.

ACKNOWLEDGEMENTS
This work was subsidized by the Fundamental Research Funds for the Central Universities (China University of Mining & Technology, Grant 2017XKZD10) and the Priority Academic Program Development of Jiangsu Higher Education Institutions.

References

1. S. Yoda, K. Ishihara, *J. Power Sources*, 68 (1997) 3.
2. H.R. Wang, S.K. Yu, B. Xu, *Chem. Commun.*, 52 (2016) 11512.
3. G.M. Luo, H.S. Li, D.Q. Zhang, L.X. Gao, T. Lin, *Electrochim. Acta*, 235 (2017) 175.
4. M. Ni, Z.H. Huang, X.L. Zhang, J.P. Liu, L. Qiao, W. Yang, *RSC Adv.*, 7 (2017) 22447.
5. E. Lim, C. Jo, J. Lee, *Nanoscale*, 8 (2016) 7827.
6. Y. Shu, J. Maruyama, S. Iwasaki, S. Maruyama, Y.H. Shen, H. Uyama, *J. Power Sources*, 364 (2017) 374.
7. W.H. Qu, Y.B. Guo, W.Z. Shen, W.C. Li, *J. Phys. Chem. C*, 120 (2016) 15105.
8. X.L. Gao, W. Xing, J. Zhou, G.Q. Wang, S.P. Zhuo, Z. Liu, Q.Z. Xue, Z.F. Yan, *Electrochim. Acta*, 133 (2014) 459.
9. V. Barranco, M. A. Lillo-Rodenas, A. Linares-Solano, A. Oya, F. Pico, J. Ibañez, F. Agullo-Rueda,

J. M. Amarilla, J.M. Rojo, *J. Phys. Chem. C,* 114 (2010) 10302.
10. H. Zhang, G.P. Cao, Y.S. Yang, *Energ. Environ. Sci.,* 2 (2009) 932.
11. J. Yan, T. Wei, B. Shao, F.Q. Ma, Z.J. Fan, M.L. Zhang, C. Zheng, Y.C. Shang, W.Z. Qian, F. Wei, *Carbon,* 48 (2010) 173.
12. B.B. Chang, Y.L. Wang, K.M. Pei, S.M. Yang, X.P. Dong, *RSC Adv.,* 4 (2014) 40546.
13. C. Kim, Y.O. Choi, W.J. Lee, K.S. Yang, *Electrochim. Acta,* 50 (2004) 883.
14. D.W. Wang, F. Li, M. Liu, G.Q. Lu, H.M. Cheng, *Angew. Chem.,* 47 (2008) 373.
15. W.D. Geng, F.W. Ma, G. Wu, S.J. Song, J.F. Wan, D. Ma, *Electrochim. Acta,* 191 (2016) 854.
16. Y. Han, X.T. Dong, C. Zhang, S.X. Liu, *J. Power Sources,* 211 (2012) 92.
17. J.N. Yi, Y. Qing, C.T. Wu, Y.X. Zeng, Y.Q. Wu, X.H. Lu, Y.X. Tong, *J. Power Sources,* 351 (2017) 130.
18. H. Peng, G.F. Ma, K.J. Sun, Z.G. Zhang, Q. Yang, Z.Q. Lei, *Electrochim. Acta,* 190 (2016) 862.
19. W.R. Feng, P. He, S.S. Ding, G.L. Zhang, M.Q. He, F.Q. Dong, J.W. Wen, L.C. Du, M.Z. Liu, *RSC Adv.,* 6 (2016) 5949.
20. C.T. Hsieh, H. Teng, *Carbon,* 40 (2002) 667.
21. Y. Chu, D. Zhang, L. Lei, Q. Yi, L. Li, *J. Hazard. Mater.,* 306 (2013) 252.
22. A.A. Elhendawy, *Carbon,* 41 (2003) 713.
23. X.J. He, H.B. Zhang, H. Zhang, X.J. Li, N. Xiao, J.S. Qiu, *J. Mater. Chem. A,* 2 (2014) 19633.
24. T. Tomko, R. Rajagopalan, P. Aksoy, H.C. Foley, *Electrochim. Acta,* 56 (2011) 5369.
25. B. Petrova, T. Budinova, N. Petrov, M.F. Yardim, E. Ekinci, M. Razvigorova, *Carbon,* 43 (2005) 261.
26. Y. Guo, Z.Q. Shi, M.M. Chen, C.Y. Wang, *J. Power Sources,* 252 (2014) 235.
27. T.T. Guan, K.X. Li, J.H. Zhao, R.J. Zhao, G.L. Zhang, D.D. Zhang, J.L. Wang, *J. Mater. Chem. A,* 5 (2017) 15869.
28. A.G.E. Daguerre , F. Stoeckli, *Carbon,* 39 (2001) 1279.
29. T. Tomko, R. Rajagopalan, M. Lanagan, H.C. Foley, *J. Power Sources,* 196 (2011) 2380.
30. H. Gao, L. Ding, H. Bai, A.H. Liu, S.Z. Li, L. Li, *J. Mater. Chem. A,* 4 (2016) 16490.
31. Y. Wu, J.P. Cao, Z.Q. Hao, X.Y. Zhao, Q.Q. Zhuang, J.S. Zhu, X.Y. Wang, X.Y. Wei, *Int. J. Electrochem. Sci.,* 12 (2017) 7227.
32. W.H. Li, Q.Y. Yue, B.Y. Gao, X.J. Wang, Y.F. Qi, Y.Q. Zhao, Y.J. Li, *Desalination,* 278 (2011) 179.
33. X.J. He, J.X. Wang, G.H. Xu, M.X. Yu, M.B. Wu, *Diam. Relat. Mater.,* 66 (2016) 119.
34. T. Wei, X. Wei, Y. Gao, H. Li, *Electrochim. Acta,* 169 (2015) 186.
35. Z.Q. Hao, J.P. Cao, X.Y. Zhao, Y. Wu, J.S. Zhu, Y.L. Dang, Q.Q. Zhuang, X.Y. Wei, *J. Colloid Interf. Sci.,* 513 (2018) 20.
36. D. Lozano-Castelló, J.M. Calo, D. Cazorla-Amorós, A. Linares-Solano, *Carbon,* 45 (2007) 2529.
37. H.F. Arani, A.R. Mirhabibi, S. Collins, R. Daroughegi, A. Khalife Soltani, R. Naghizadeh, N. Riahi-Noori, R. Aghababazadeh, A. Westwood, *RSC Adv.,* 7 (2017) 5533.
38. M.A. Nahil, P.T. Williams, *Biomass Bioenerg.,* 37 (2012) 142.
39. R. Farma, M. Deraman, A. Awitdrus, I.A. Talib, E. Taer, N.H. Basri, J.G. Manjunatha, M.M. Ishak, B.N. Dollah, S.A. Hashmi, *Bioresource Technol.,* 132 (2013) 254.
40. P. Liu, J.R. Kong, Y.R. Liu, Q.C. Liu, H.Z. Zhu, *J. Power Sources,* 278 (2015) 522.
41. D. Puthusseri, V. Aravindan, S. Madhavi, S. Ogale, *Energ. Environ. Sci.,* 7 (2014) 728.
42. J.C. Wang, S. Kaskel, *J. Mater. Chem.,* 22 (2012) 23710.
43. T. Otowa, R. Tanibata, M. Ltoh, *Gas Separat. Purificat.* 7(1993) 241.
44. C. Bouchelta, M.S. Medjram, O. Bertrand, J.P. Bellat, *J. Anal. Appl. Pyrol.,* 82 (2008) 70.
45. Q. Zhang, K.H. Han, S.J. Li, M. Li, J.X. Li, K. Ren, *Nanoscale,* 10 (2018) 2427.
46. F. Zhang, T.Y. Liu, M.Y. Li, M.H. Yu, Y. Luo, Y.X. Tong, Y. Li, *Nano Lett.,* 17 (2017) 3097.
47. N.N. Guo, M. Li, X.K. Sun, F. Wang, R. Yang, *Green Chem.,* 19 (2017) 2595.
48. M.S. Park, S. Cho, E. Jeong, Y.S. Lee, *J. Ind. Eng. Chem.,* 23 (2015) 27.
49. J.G. Wang, Y. Yang, Z.H. Huang, F.Y. Kang, *Carbon,* 61 (2013) 190.

50. J. Chmiola, G. Yushin, Y. Gogotsi, C. Portet, P. Simon, P.L. Taberna, *Sci.*, 313 (2006) 1760.
51. D. Hulicova-Jurcakova, M. Kodama, S. Shiraishi, H. Hatori, Z.H. Zhu, G.Q. Lu, *Adv. Funct. Mater.*, 19 (2009) 1800.
52. Q. Li, R.R. Jiang, Y.Q. Dou, Z.X. Wu, T. Huang, D. Feng, J.P. Yang, A.S. Yu, D.Y. Zhao, *Carbon*, 49 (2011) 1248.
53. E. Frackowiak, F. Begui, *Carbon*, 39 (2001) 937.
54. Z.Q. Hao, J.P. Cao, Y. Wu, X.Y. Zhao, Q.Q. Zhuang, X.Y. Wang, X.Y. Wei, *J. Power Sources*, 361 (2017) 249.
55. R.J. Mo, Y. Zhao, M. Wu, H.M. Xiao, S. Kuga, Y. Huang, J.P. Li, S.Y. Fu, *RSC Adv.*, 6 (2016) 59333.
56. Y. Wu, J.P. Cao, X.Y. Zhao, Z.Q. Hao, Q.Q. Zhuang, J.S. Zhu, X.Y. Wang, X.Y. Wei, *Electrochim. Acta*, 252 (2017) 397.
57. X.Y. Zhao, S.S. Huang, J.P. Cao, S.C. Xi, X.Y. Wei, J. Kamamoto, T. Takarada, *J. Anal. Appl. Pyroly.*, 105 (2014) 116.
58. X.Y. Zhao, S.S. Huang, J.P. Cao, X.Y. Wei, K. Magarisawa, T. Takarada, *Fuel Process. Technol.*, 125 (2014) 251.
59. L. Jiang, J.W. Yan, L.X. Hao, R. Xue, G.Q. Sun, B.L. Yi, *Carbon*, 56 (2013) 146.